Links between marine and atmospheric processes oscillating on a millennial time-scale. A multi-proxy study of the last 50,000 yr from the Alboran Sea (Western Mediterranean Sea)

Ana Moreno[a,b,*], Isabel Cacho[b,c], Miquel Canals[b], Joan O. Grimalt[d], María Fernanda Sánchez-Goñi[e], Nick Shackleton[c], Francisco J. Sierro[f]

[a]*Pyrenean Institute of Ecology, Spanish Research Scientific Council, Avda. Montañana 1005, 50080 Zaragoza, Spain*
[b]*CRG Marine Geosciences, Department of Stratigraphy, Paleontology and Marine Geosciences, Faculty of Geology, University of Barcelona, Campus de Pedralbes, C/Martí i Franqués, s/n°, E-08028 Barcelona, Spain*
[c]*University of Cambridge, The Godwin Laboratory, Pembroke Street, Cambridge CB2 3SA, UK*
[d]*Department of Environmental Chemistry, Institute of Chemical and Environmental Research (CSIC), Jordi Girona, 18, 08034 Barcelona, Spain*
[e]*EPHE, Département Géologie et Océanographie, UMR-CNRS 5805, University Bordeaux 1, France*
[f]*Department of Geology, University of Salamanca, Plaza de la Merced s/n. 37008, Salamanca, Spain*

Abstract

The large dataset obtained from the extensive study of IMAGES core MD95-2043 recovered from the Alboran Sea (Western Mediterranean) shows the periodicities and phase relationships of oceanographic and atmospheric processes on a millennial time-scale. The 1470-yr cycle is the most significant, with the exception of the records reflecting climatic or environmental changes on land which show statistically significant 3300 and 8000 frequency bands. The investigation of these core records on a millennial scale resolution allows us to establish the evolution of oceanographic and atmospheric mechanisms that influenced the Western Mediterranean region in the course of the Dansgaard/Oeschger cycles. Accordingly, possible land–sea interactions can be identified and situated in the context of the temporal succession of the different climatic processes. For instance, Saharan dust supply from Northern Africa appears to lead high-latitude climate changes, suggesting that low-latitude feedback processes were involved in forcing the millennial climatic variability in the westernmost Mediterranean.
© 2005 Elsevier Ltd. All rights reserved.

1. Introduction

During the last decade many paleoclimate studies have focused on the high-frequency climatic instabilities during the last glacial period, known as the Dansgaard/Oeschger (D/O) cycles (Bond et al., 1993; Dansgaard et al., 1993). These climate fluctuations are present in numerous marine and continental records all over the world (Leuschner and Sirocko, 2000; Voelker, 2002), demonstrating the global impact of this rapid variability. To further understand the ultimate implications of such rapid variability, we need to identify the different marine and atmospheric processes involved in these changes in order to elucidate how they propagated between various regions and latitudes. One major, but still unsolved, aspect concerns the time relationship between these processes, since this information may offer clues for understanding the forcing mechanisms that triggered the D/O cycles. Making progress in this line of research will require: (1) high-resolution proxy profiles from paleoclimate archives that record simultaneously oceanographic and atmospheric processes; (2) a focus on highly sensitive areas that provide a clear signal of these abrupt climate changes; and (3) an

*Corresponding author. Pyrenean Institute of Ecology, Spanish Research Scientific Council, Avda. Montañana 1005, 50080 Zaragoza, Spain. Tel.: +34 976 716118; fax: +34 976 716019.

E-mail address: amoreno@ipe.csic.es (A. Moreno).

analysis of key regions which can integrate data from processes running at different latitudes, thus offering information on their potential linking and timing.

The Mediterranean Sea fulfills these requirements. Due to its semi-enclosed character and its hydrographic characteristics it is very sensitive to climatically induced environmental changes and, because of its geographical position, the whole region is influenced by both high- and low-latitude climatic systems (Krijgsman, 2002; Cacho et al., 2002). One of the most extensively studied cores from the Western Mediterranean is IMAGES core MD95-2043, recovered from the Alboran Sea, which has permitted the identification of several oceanographic and atmospheric processes (Cacho et al., 1999, 2000, 2001, 2002; Bárcena et al., 2001; Moreno et al., 2002, 2004; Sánchez-Goñi et al., 2002; Pérez-Folgado et al., 2003). The high sedimentation rates of this core (over 25 cm/kyr for most of the glacial interval) have allowed the study of past environmental changes on a centennial time-scale. Studies of this core demonstrated an extremely high correlation coefficient ($r = 0.92$) between Greenland ice $\delta^{18}O$ and Alboran sea surface temperature (SST) records over the last 50 kyr (Cacho et al., 1999), thus proving the existence of a strong link between these two regions. Further work using several different proxies has shown that high frequency variability was reflected not only in SST but also in many other parameters controlled by both oceanic and atmospheric processes (Moreno et al., 2002; Sánchez-Goñi et al., 2002). The comparison of terrestrial and marine proxy data from the same core significantly reduces the dating uncertainties that are normally encountered in studies in which records of this kind are derived from several cores or archives. So core MD95-2043 provides a unique dataset for the exploration of the interactions between different mechanisms which are likely to oscillate on the millennial–centennial time-scale, and their timing relationship.

The present study summarizes previous analytical work on different oceanic and atmospheric proxies measured from this core evaluated together in order to elucidate their temporal sequencing. This integrated study aims to discuss the variability of the different proxies in the context of two main climatic and oceanic scenarios that oscillated at the D–O frequency and to analyze their timing, dominant frequency and phase relationship in order to identify potential leads and lags between climatic and environmental processes. Statistical analyses were used to identify and interpret the different patterns of variation on the millennial time-scale in order to assess the climatic scenarios inferred for the D/O cycles in the Mediterranean region.

2. Core location, present-day oceanography and climate

Core MD95-2043 was retrieved from the Alboran Sea, the westernmost basin in the Mediterranean Sea, (36° 8.6′N;

2° 37.3′W; 1841 m water depth) during the 1995 IMAGES-I Calypso coring campaign onboard *R/V Marion Dufresne* (Fig. 1a). The Mediterranean Sea acts as a concentration basin in which evaporation exceeds fresh water input through precipitation and runoff (Béthoux, 1979). This semi-enclosed sea is characterized by a complete thermohaline circulation system, involving surface water entrance from the North Atlantic Ocean, in situ densification by air–sea interaction and deep outflowing to the Atlantic through the Alboran Sea (Pinardi and Masetti, 2000). Three water masses fill the Alboran basin: the surface layer called the Modified Atlantic Water (MAW) which describes two anticyclonic gyres; the intermediate water, a relict of the Levantine Intermediate Water (LIW) formed in the Eastern Mediterranean and, finally, the Western Mediterranean Deep Water (WMDW) produced in the Gulf of Lions (Fig. 1b) where north-westerly winds evaporate and cool the surface water until it sinks to the deep basin (Perkins et al., 1990; Millot, 1999).

The summertime Mediterranean climate is usually dry and hot due to the influence of the atmospheric subtropical high-pressure belt (Sumner et al., 2001). During winter the subtropical high shifts southwards, allowing mid-latitude storms to enter the region from the open Atlantic, which bring greater amounts of rainfall to the Mediterranean. Much of the present-day climate variability in this region on a decadal time-scale has been linked to the North Atlantic Oscillation (NAO; Rodó et al., 1997). During low NAO index years, north-westerly winds are weaker and guided to mid-latitudes, bringing higher precipitation to the Mediterranean and North African areas; during high NAO index years, the strong meridional pressure gradient leads to a more northerly route of the North Atlantic depression tracks, thus bringing humidity to central and northern Europe.

3. Methodology

The chronological framework of core MD95-2043 is described and discussed in Cacho et al. (1999). According to the age model, the core section studied here, from 1025 to 1585 cm core depth, spans the time interval 28,000 and 48,000 cal. yr BP. Sedimentation rates are 27 cm/kyr on average, resulting in a temporal resolution of our records of 185 years at sampling intervals of 5 cm (see also Moreno et al., 2003). The section studied starts below a depth of 10 m of sediment, which is the maximum depth of stretching identified by Skinner and McCave (2003).

The main proxies included in this study and the analytical methods used for their measurement were as follows:

i) Stable isotopes on the planktic and benthic foraminifera determined using a SIRA mass spectrometer equipped with a VG isocarb common acid bath system (Cacho et al., 1999, 2000).
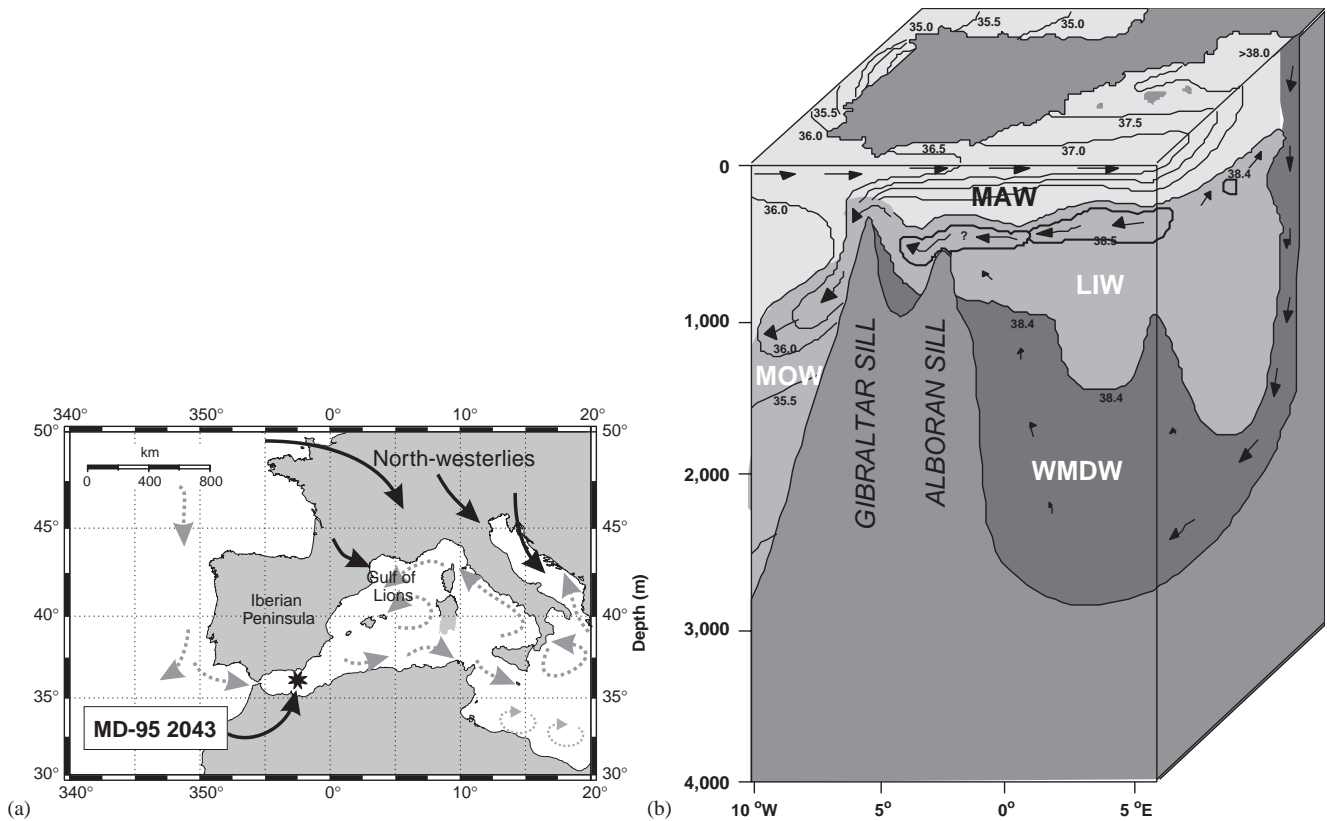
Fig. 1. (a) Location of IMAGES core MD95-2043 in the Alboran Sea. Present-day dominant oceanographic circulation is represented by dashed arrows. (b) A 3D illustration of the water masses circulation in the Western Mediterranean Sea indicated by black arrows. Salinity values are also shown.

ii) Molecular biomarkers (long-chain alkenones, alkanes, alcohols) analyzed with a Varian gas chromatograph Model 3400 equipped with a septum programmable injector and flame ionization detection (Cacho et al., 1999, 2000).

iii) Relative proportion of *Neogloboquadrina pachyderma* (s) in total planktonic foraminifera counted in the sample (Cacho et al., 1999).

iv) Total organic carbon content determined with a Carlo-Erba (NA 1500) Elemental Analyser (Cacho et al., 2000).

v) Grain-size analyses of the terrigenous fraction measured with a Coulter Laser Sizer (LS 100) (Moreno et al., 2002).

vi) Content in bulk major (Na, Mg, Al, Si, P, K, Ca, Ti, Mn and Fe) and trace elements (Sn, Nb, Zr, Y, Rb, Th, Ga, Zn, Cu, Ni, V, Ce, Co, Pb, Ba and Cr) obtained by means of X-ray fluorescence (XRF) with a Philips PW 2400 sequential wavelength dispersive X-ray spectrometer (Moreno et al., 2002).

vii) Pollen preparation and counting as described in Sánchez-Goñi et al. (2002).

The proxy records were resampled in order to obtain a uniform 150-year interval for the period under consideration (28–48 kyrs), which is close to the mean temporal resolution of the records before carrying out the spectral analyses. To extract significant periodicities, spectral analysis was performed using some of the methods provided by the AnalySeries software package (Paillard et al., 1996): Blackman-Tukey, Multi-Taper and Maximum Entropy Methods. The Multi-Taper Method is the principal tool in spectrum estimation here, since it allows detection of low-amplitude oscillations in short time series with a high degree of statistical significance (Yiou et al., 1996). It also provides a narrow band F-test for the presence and significance of periodic components that do not depend on the magnitude of power (Thomson, 1990). As for the SST spectral record, the cyclicities are defined by the age model construction, e.g., the SST record is tuned to the GISP2 $\delta^{18}O$ record. However, proxies that were not used for tuning the age model provide statistically independent records (Tables 1 and 2). Once the main frequency bands were extracted from the proxy records, leads and lags between those with a D/O periodicity were calculated in the time domain (Table 3). We compared the time at which the proxies analyzed reached minimum and maximum, in order to establish the sequence of the different processes.

Table 1
Results of spectral analyses carried on selected proxies from core MD95-2043 and compared with those from GISP2 records

	Process	Variable	Frequency bands				Ref
			≈ 8000 yr	5000 yr	3300 yr	1470 yr	
Greenland GISP2	Temperature	$\delta^{18}O$	—	5535; 0.87	3350; 0.86	**1462; 0.99**	a
	Atmospheric circulation	PCI	—	**5250; 0.97**	3350; 0.91	**1462; 0.99**	b
Alboran Sea MD95-2043	SST	SST (°C)	—	5485; 0.93	3200; 0.91	**1462; 0.98**	c
		N. pachyderma	7680; 0.93	—	—	—	c
	Productivity	Ba_{excess} (ppm)	—	6407; 0.83	**3334; 0.95**	1570; 0.86	d
		Alkenones (ng/g)	—	—	3350; 0.92	**1484; 0.97**	e
		TOC (%)	—	5250; 0.87	3413; 0.90	**1494; 0.96**	e
		$CaCO_3$ (%)	—	—	3200; 0.94	**1402; 0.98**	d
	Deep-water conditions	$\delta^{13}C$ (benthics)	—	—	**3470; 0.99**	**1412; 0.98**	d,e
		n-hexacosanol/*n*-nonacosane index	—	**5119; 0.96**	—	**1462; 0.98**	e
	Aridity Iberia	Steppics (%)	9300; 0.91	—	3011; 0.93	1484; 0.86	f
		Aluminium (%)	—	—	3413; 0.91	1422; 0.85	g
	Saharan winds	Si/(Si + K)	—	—	**3134; 0.99**	1505; 0.84	g
		End-member 1	**7680; 0.99**	—	—	1383; 0.83	g

The predefined "*compromise*" level was used (bandwidth = 0.66; no. windows = 6). Frequency bands are selected from the amplitude peaks obtained from the MTM (Fig. 4). The amplitude peak (in years) and the value of *F*-test (from 0 to 1) are shown. No spectral variance at a selected frequency band is indicated by (—). Intervals with *F*-test > 0.95 are considered significant (in bold type).
References where the records were published are shown (Ref). a—Grootes and Stuiver (1997); b—Mayewski et al. (1997);c—Cacho et al. (1999);d—Moreno et al. (2003);e—Cacho et al. (2000);f—Sánchez-Goñi et al. (2002);g—Moreno et al. (2002).

Table 2
Percentage of variance explained by the statistically significant band-components of each proxy considered in the study

	Process	Variable	Frequency bands				Ref
			≈ 8000 yr	5000 yr	3300 yr	1470 yr	
Greenland GISP2	Temperature	$\delta^{18}O$	—	16.3	21.68	31.87	a
	Atmospheric circulation	PCI	—	19.61	20.68	32.6	b
Alboran Sea MD 95-2043	SST	SST (°C)	—	29.68	31.63	15.64	c
		N. pachyderma	25.01	—	—	—	c
	Productivity	Ba_{excess} (ppm)	—	22.15	27.11	18.39	d
		Alkenones (ng/g)	—	—	21.87	22	e
		TOC (%)	—	28.95	16.9	19.77	e
		$CaCO_3$ (%)	—	—	26.07	21.02	d
	Deep Water Conditions	$\delta^{13}C$ (benthics)	—	—	34.43	12.18	d,e
		n-hexacosanol/*n*-nonacosane index	—	13.42	—	29.96	e
	Aridity/humidity Iberia	Steppics (%)	25.33	—	23.72	15.96	f
		Aluminium (%)	—	—	23.9	18.65	g
	Saharan winds	Si/(Si + K)	—	—	30.85	13.17	g
		End-member 1	22.76	—	—	13.91	g

References where the records were published are shown (Ref). a—Grootes and Stuiver (1997);b—Mayewski et al. (1997);c—Cacho et al. (1999);d—Moreno et al. (2003);e—Cacho et al. (2000);f—Sánchez-Goñi et al. (2002);g—Moreno et al. (2002).

4. D/O variability of the last glacial period in the Mediterranean region

D/O variability in the Mediterranean Sea was first identified in a SST record based on alkenone analyses from Alboran Sea core MD95-2043 (Cacho et al., 1999).

Alkenone data in this study were completed with a record of the polar foraminifer *N. pachyderma* (s) which confirmed that the most severe cold conditions occurred during those D/O stadials associated with the North Atlantic Heinrich events (HE) (Fig. 2c,d). Changes in the North Atlantic thermohaline circulation are

Table 3
Phase relationships of proxy records from IMAGES core MD95-2043 during a D/O cycle calculated for the time to reach the coldest and warmest events and the inflexion point from cold to warm abrupt event

Average phase difference (kyr); standard deviation (kyr)

Variable vs. SST	Time to reach the coldest event	Time to reach the warmest event	Time to reach the inflexion point from cold to warm abrupt event
Ba_{excess} (ppm) vs. SST	0.27; 0.31	0.25; 0.28	0.21; 0.2
Alkenones vs. SST	0.07; 0.31	0.08; 0.27	0.37; 0.48
TOC (%) vs. SST	0.12; 0.27	0.19; 0.24	0.26; 0.22
$CaCO_3$ (%) vs. SST	0.56; 0.30	0.29; 0.32	0.47; 0.26
$\delta^{13}C$ (benthics) vs. SST	0.24; 0.31	−0.12; 0.48	0.21; 0.23
Alcohol index vs. SST	0.12; 0.26	−0.22; 0.51	0.07; 0.15
Steppics vs. SST	−0.20; 0.24	−0.42; 0.57	−0.21; 0.17
Al (%) vs. SST	−0.44; 0.49	−0.54; 0.56	−0.37; 0.36
Si/Si + K vs. SST	−0.26; 0.43	−0.33; 0.25	−0.22; 0.28

Average phase differences among SST and other proxies and the standard deviation are shown in 10^3 years (positive values indicate that SST leads the other proxy). See Fig. 5 for a graphic representation.

considered responsible for the entrance of a cold, polar source, surface water mass from the Atlantic into the Mediterranean at the time of these D/O stadials. These results were confirmed by foraminifera assemblage SST reconstructions from the same core, the nearby core ODP977 (Pérez-Folgado et al., 2003) and a dinoflagellate and pollen record from core ODP976 also in the Alboran Sea (Combourieu Nebout et al., 2002). SST cooling during some of the HE has been recognised in other basins in the Western Mediterranean Sea such as the Tyrrhenian Sea (Paterne et al., 1999; Cacho et al., 2001) and the Gulf of Lions (Rohling et al., 1998) where changes in the intensity and position of the north-westerly winds are reported to be among the mechanisms responsible for these rapid coolings.

Identification of past changes in primary productivity is always complex due to the many factors which may potentially affect the different proxies. Organic matter records from core MD95-2043 such as total organic carbon and total C_{37} alkenone content were published by Cacho et al. (2000). However, these records were only discussed in terms of primary productivity after an exhaustive comparison with other primary productivity records such as calcium carbonate and barium excess (Ba_{excess}) profiles and in combination with redox-sensitive elements to separate the true productivity signals from those that are derived from diagenetic modifications (Moreno et al., 2003). As a result, the D/O related primary productivity variability has been characterized consisting of higher values during the D/O warm interstadials than during the stadials (Fig. 2e,f). This enhanced interstadial primary productivity activity is believed to have been led by a persistent southward shift of the westerly winds to the latitude of the Alboran Sea which forced a more energetic inflowing of Atlantic surface jet and led to increased gyre-induced upwelling

of nutrient-rich subsurface water. Wind-driven changes in past primary productivity in the Alboran Sea have been discussed elsewhere, but only with reference to the time of the last deglaciation (Abrantes, 1988; Vergnaud-Grazzini and Pierre, 1991; Bárcena et al., 2001).

At the core depth studied (1841 m) sediments are under the influence of the WMDW which is formed in the northern area of the Gulf of Lions (Fig. 1, and see Section 2). Both $\delta^{13}C$ (Fig. 2g) and $\delta^{18}O$ records from the benthic foraminifer *Cibicidoides pachyderma* show relatively large oscillations in parallel to the D/O variability (Cacho et al., 2000). These data are believed mainly to represent changes in the ventilation rate and in the properties of the deep water involving that the convection of WMDW was more efficient during the cold D/O stadials than the interstadials (Cacho et al., 2000; Moreno et al., 2003). These interpretations are further supported by an alternative record, the *n*-hexacosanol/*n*-nonacosane index (Fig. 2h, which reflects the relative concentration of two terrestrial source molecular biomarkers with different chemical stability vs. oxidation). In the particular context of the Alboran Sea, high values (D/O interstadials) are taken to indicate better preservation conditions of the organic matter resulting from decreased deep-water ventilation (Cacho et al., 2000). The benthic foraminifer assemblage was also very sensitive to these oscillations, confirming the dominance of well-ventilated/oxygenated conditions during the D/O stadials (I. Reguera, personal communication). These D/O oscillations in the rate of WMDW convection result from changes in the intensity of the north-westerly winds over the Gulf of Lions (Cacho et al., 2000).

Climate conditions over southern Iberia have also been studied in core MD95-2043 by means of the pollen content and geochemical analysis (Sánchez-Goñi et al.,
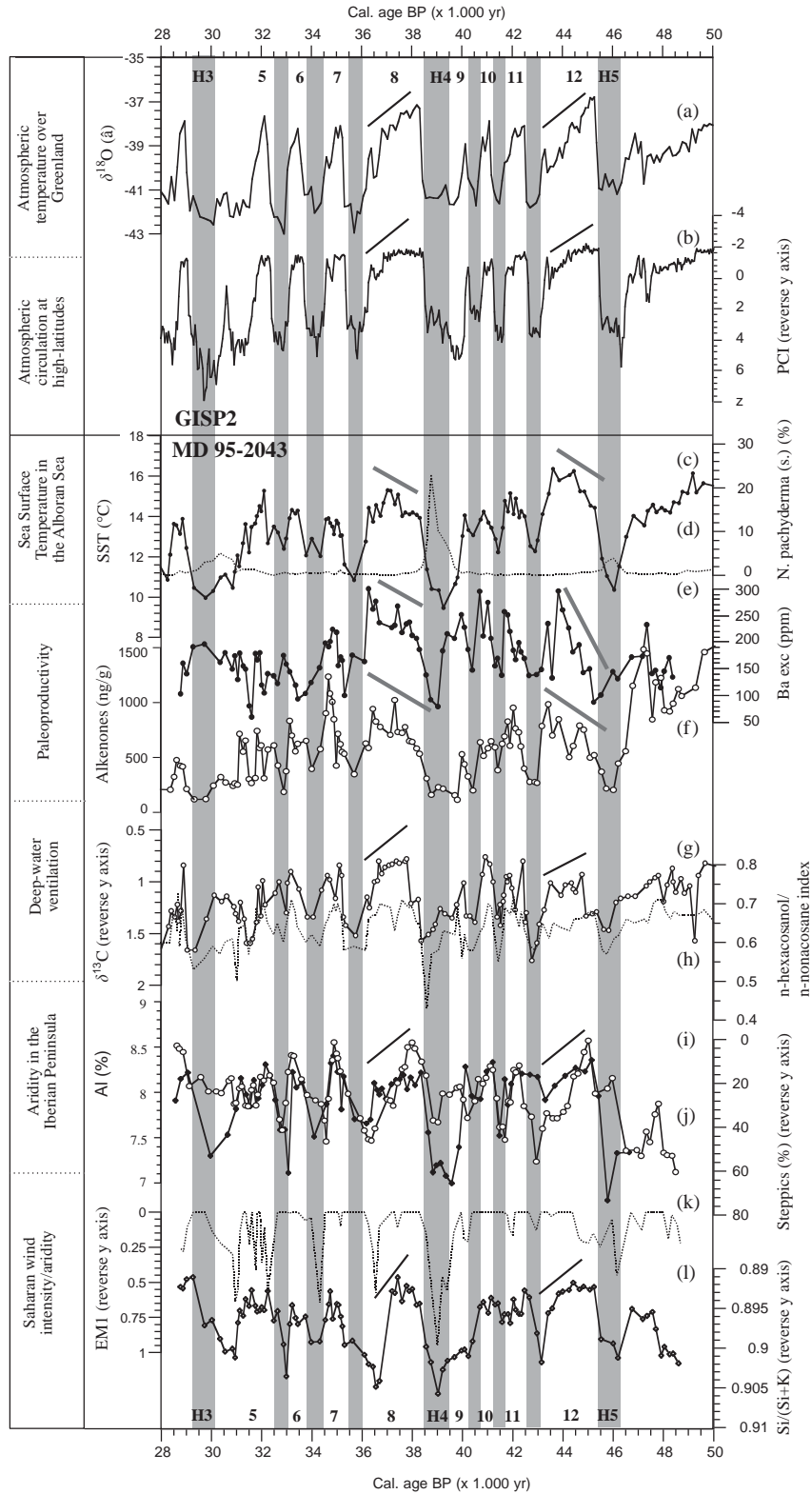
Fig. 2. Comparison of different proxies selected from core MD95-2043 and ice core GISP2: (a) $\delta^{18}O$ and (b) PCI from GISP2 (Grootes and Stuiver, 1997; Mayewski et al., 1997); (c) $U^{k'}_{37}$-SST (Cacho et al., 1999); (d) % of *N. pachyderma* (s.) (dashed line) (Cacho et al., 1999); (e) Ba_{excess} (Moreno et al., 2003); (f) Alkenone total concentration (ng/g) (white dots) (Cacho et al., 2000); (g) $\delta^{13}C$ (benthics) (reverse *y*-axis) (Moreno et al., 2003); (h) *n*-hexacosanol/*n*-nonacosane index (dashed line) (Cacho et al., 2000); (i) steppic vegetation (black dots, reverse *y*-axis) (Sánchez-Goñi et al., 2002); (j) Aluminium percentage (white dots) (Moreno et al., 2003); (k) EM1 relative abundance (Moreno et al., 2002) and (l) Si/(Si + K) (Moreno et al., 2002) from MD95-2043 core. Processes represented are indicated in the left-hand boxes. Black and gray lines are plotted to illustrate the differences in interstadial evolution (D/O interstadials 8 and 12) between atmospheric and marine systems.

2002; Moreno et al., 2002). The results suggest that the vegetation cover shifted drastically from the dominance of steppic plants during the D/O stadials, in particular those associated to the HE, to more forest development during D/O interstadials (Fig. 2i, reverse y axis). The pollen reconstruction is also consistent with other similar reconstruction from marine cores from the Alboran Sea (Combourieu Nebout et al., 2002) and the western Iberian margin (Roucoux et al., 2001; Sánchez-Goñi et al., 2002) and other Mediterranean lake sequences from southern Italy (Allen et al., 1999) and Greece (Tzedakis et al., 2002). More humid conditions during the D/O interstadials, with enhanced runoff towards the Alboran Sea, are also suggested by the aluminum content record (Fig. 2j).

The Alboran Sea is located under the path of the high-altitude northward winds which transport Saharan dust towards the European continent. To analyze potential changes in the transport of Saharan dust towards these northern latitudes during the time of the D/O variability, the Si/(Si + K) ratio and an end member model from the size fraction distribution (Fig. 2k, l) were measured in core MD95-2043 as indicators of the terrigenous fraction of Saharan origin (Moreno et al.,

2002). The results indicate stronger Saharan dust transport during the cold D/O stadial periods (Moreno et al., 2002).

The combination of all these data provides parallel information about several different marine (SST, primary productivity, deep-water convection) and atmospheric processes (north-westerly system, Saharan winds, humidity over southern Iberia) whose variability can be compared within the time resolution of our sampling interval (about 150 years). Two distinct scenarios representing D/O stadials and interstadials can be defined with these proxy records (Fig. 3). Cold D/O events (stadials) and HE were defined by lower SST and higher aridity due to more vigorous north-westerly winds over the northwestern Mediterranean and Saharan winds involving a more efficient meridional dust transport. In contrast, D/O interstadials were characterised by warmer temperatures, higher continental humidity and increased primary productivity in the Alboran Sea as a consequence of a southward shift in the north-westerlies. In addition, paleoceanographic data and climatic models indicate the occurrence of strong SST and atmospheric pressure gradients in the North Atlantic during the D/O stadials (Ganopolski
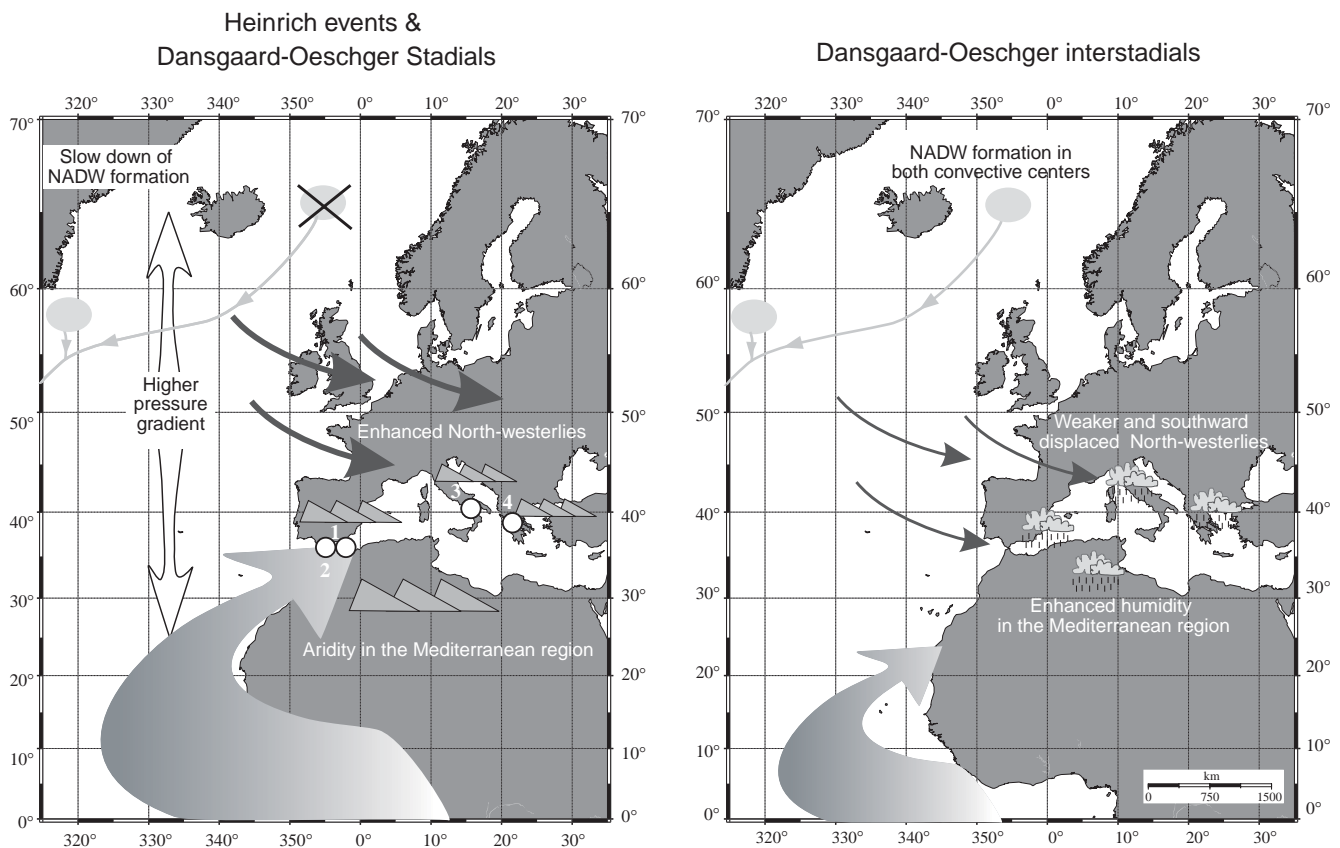
Fig. 3. D/O scenarios that summarize the main processes and features that controlled the Alboran record during HE and D/O stadial (a) and D/O interstadial periods (b). Numbers from 1 to 4 in the figure correspond to the following cores: 1: MD95-2043 (Cacho et al., 1999); 2: ODP976 (Combourieu Nebout et al., 2002); 3: Lago Grande di Monticchio (Allen et al., 1999); 4: Kopais basin (Tzedakis et al., 1999).

and Rahmstorf, 2001; Voelker, 2002), whereas in the D/O interstadials (Fig. 3b), the lowered pressure gradient along the North Atlantic gave rise to a semi-permanent low-pressure system in the Mediterranean region. These changes in the North Atlantic atmospheric pressure gradient bear similarities to the present-day NAO. Although the resolution of core MD95-2043 cannot monitor the millennial behavior of the NAO, and the boundary conditions during glacial times were very different from those of the present day, several parallels between the D/O oscillation mode of the processes mentioned above and present-day NAO variability can be drawn (Hurrell, 1995; Wanner et al., 2001). Some studies have considered that these D/O cycles could be explained as the glacial operation of a NAO-like mechanism oscillating on a millennial time-scale (Combourieu Nebout et al., 2002; Moreno et al., 2002; Sánchez-Goñi et al., 2002).

5. Frequency and phase relationships between the different proxies and their implications

The proxy records mentioned above (Fig. 2) provide a wide range of information on atmospheric and oceano-graphic processes in the context of the D/O climatic variability. Now, periodicities and phase relationships will be examined for the following selected parameters: (i) Alboran SST, inferred from the $U_{37}^{k'}$ index and the percentage of *N. pachyderma* (s.) (Cacho et al., 1999), (ii) primary productivity, reflected by the concentration of Ba_{excess}, TOC and alkenones (Cacho et al., 2000; Moreno et al., 2003), (iii) deep-water ventilation, indicated by benthic $\delta^{13}C$ and the *n*-hexacosanol/*n*-nonacosane index, (iv) aridity/humidity in the southern Iberian Peninsula, obtained from the abundance of steppic vegetation pollen (Sánchez-Goñi et al., 2002) and the percentage of Al (Moreno et al., 2003), and (v) Saharan winds/Northern African aridity represented by the $Si/(Si + K)$ ratio as an indicator of dust supply, and the percentage of end-member 1 (EM1) in the grain-size distribution of the sediments (Moreno et al., 2002). For comparison, spectral analyses were also performed with the same statistical methods as in two GISP2 records: the $\delta^{18}O$ as indicator of the atmospheric temperature over Greenland (Grootes and Stuiver, 1997) and the Polar Circulation Index as proxy for atmospheric circulation at high latitudes (Mayewski et al., 1997).

5.1. Analyses in the frequency domain of the sub-Milankovitch bands

The use of the Multi-Taper method has shown four dominant cyclicities (F-test > 0.95) at ≈ 8000, 5000, 3300 and 1470 years (Fig. 4a, Table 1). These periodicities also occur in paleoclimatic records from high latitudes

(Grootes and Stuiver, 1997; Mayewski et al., 1997; Van Kreveld et al., 2000) and monsoon regimes (Sirocko et al., 1996; de Garidel-Thoron et al., 2001). The concurrence of these cyclicities in these two areas suggests links between the Western Mediterranean and higher latitude climatic systems, or a similar forcing mechanism. However, the proxies present differences in terms of statistical significance and percentage of explained variance (Table 2).

The 8000-yr cycle is significant for *N. pachyderma* (s.), grain-size end-member 1 and steppic vegetation abundance (Fig. 4a and Table 1). This cyclicity closely follows the periodicity of HEs in the northern North Atlantic, and its presence in our Alboran Sea records is a clear indication that changes in environmental conditions there were most severe during these events, particularly with regard to SST and aridity in the nearby borderlands. As described in the models of Ganopolski and Rahmstorf (2001), the extreme SST decreased during the HE, compared with the D/O coolings that occurred outside the immediate "Heinrich belt". It is suggested that at the start of an HE the circulation is already in the stadial mode, and that Greenland is already cold and beyond the reach of the conveyor belt, so there is hardly any further cooling there. However, in the records located further south, when a HE starts, the drop in the interhemispheric heat transport is dramatic and the resulting cooling is augmented. On the other hand, the amplified HE steppic vegetation signal by comparison with the one recorded in the other D/O stadials is a singular feature in the Mediterranean region (Combourieu Nebout et al., 2002; Sánchez-Goñi et al., 2002) since it is not identified in similar pollen records, not even those from the Atlantic margin of Iberia (Sánchez-Goñi et al., 2000; Roucoux et al., 2001). It was hypothesized that the differences in behavior of the vegetation in the Mediterranean and the Atlantic Iberian side could result from the dominance of the Scandinavian Mobile Polar Highs during HE (Sánchez-Goñi et al., 2002) whereas the Atlantic Polar High may dominate during the other stadials (Leroux, 1993). Thus, the HE meterological situation could involve a more effective aridification of the Mediterranean region of the Iberian Peninsula than in the area of Atlantic influence. The 8000-yr cyclicity in the grain size end member 1 proxy, which is also related to aridity, is consistent with this hypothesis (Table 1).

The 5000-yr cycle that is significant in the polar circulation index record of Greenland is also statistically robust in the MD95-2043 records of the *n*-hexacosanol/*n*-nonacosane index (Table 1). This agreement further supports the existence of a strong link between the rates of deep-water ventilation and the intensity of high-latitude atmospheric circulation reflected in the Greenland polar circulation index. Accordingly, it was hypothesized that the *n*-hexacosanol/*n*-nonacosane index record from the
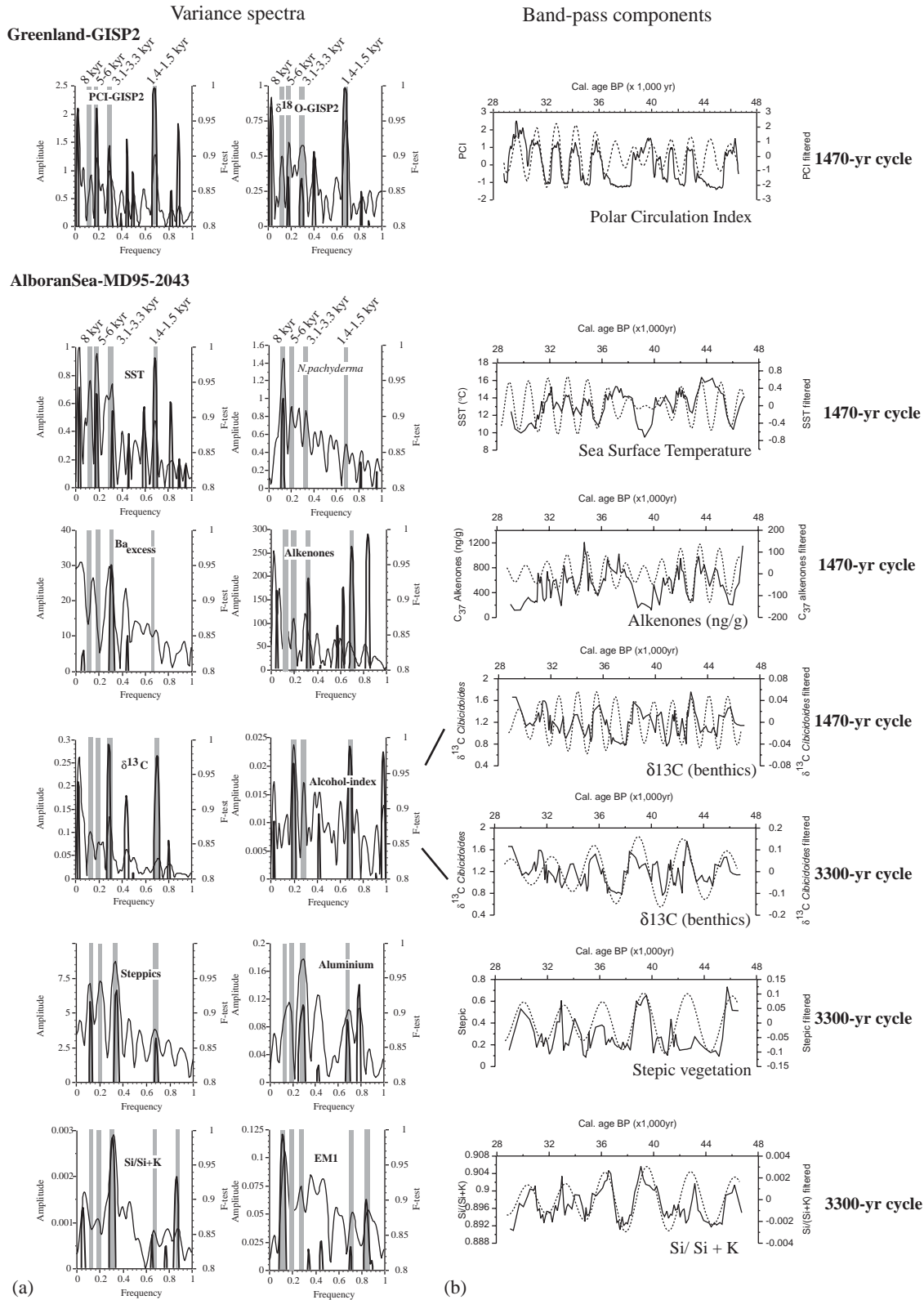
Fig. 4. (a) Variance spectra of selected records from IMAGES core MD95-2043, expressed as the line amplitude vs. frequency in cycles kyr-1 using the MTM (thinner curve) (Paillard et al., 1996). *F*-test values are also plotted (thicker line). The predefined "*compromise*" level was used (bandwidth = 0.66; no. windows = 6). The 8000, 5000, 3300 and 1470-yr cycles are marked as vertical gray bands in all the records. See Table 1 for the accurate time when the spectral peaks occur and the value of the statistical test. (b) Band-pass component filtered from a 150-year sampling of some selected series from the Alboran core MD95-2043 using a gaussian filter with central periods at 3300 years and 1470 years (dashed lines) compared with the original series (unbroken lines). See Table 2 for percentage values of the variance explained by each frequency.

Alboran Sea may monitor changes in the deep-water convection produced in the Gulf of Lions which, in turn, are directly influenced by the intensity of north-westerly winds that blow from the European continent (Cacho et al., 2000).

The 3300-yr periodicity contained in most marine and continental records from MD95-2043 and also in the GISP2 δ^{18}O and polar circulation index records (Fig. 4a and Table 1) contributes to the highest percentage of the down-core variance (Table 2). Comparison of these records with their band-pass components shows that the 3300-yr cycle is related to the presence of the prominent and prolonged D/O interstadials 8 and 12 (Fig. 4b). The presence of this 3300-yr cycle is particularly well represented in the proxies that describe the terrestrial system: intensity of the different wind systems and continental aridity. Therefore, even though this high variance contribution may reflect the better representation in the sedimentary record of the relevant processes, it is conceivable that the prolonged duration of these interstadials favored a more pronounced reorganization of the climatic subsystems monitored by our proxies.

The main period observed in the ice-core records is the 1470-yr cycle, which is also the cycle that has the highest degree of significance for most proxies in the core MD95-2043 records. The presence of this periodicity in MD95-2043 SST may be related to the tuning of this record to the GISP2 δ^{18}O. But even though F-test values and the amount of variability explained by this frequency are high for most of the other proxies, the variance associated with this cycle is lower than that of the 3300-yr cycle (Table 2). The 1470-yr periodicity is less significant in our terrestrial indicator records when compared to SST or the paleoproductivity proxies, thus suggesting that the influence of the rapid D/O climatic swings on the terrestrial system (e.g. aridity, wind systems) was much lower than on the marine environment of the Alboran Sea (Table 2).

5.2. Leads and lags calculations between the different processes

Although all MD95-2043 proxy records selected for the spectral analysis show a clear D/O variability, detailed analysis of their internal structure and relative timing show differences that may in turn reflect differences in the response of the processes that they represent. Specifically, the temperature evolution during D/O interstadials in the Alboran Sea is different. This contrast is notably defined in interstadials 8 and 12 as indicated by the black lines over the proxies in Fig. 2. SST in the Alboran Sea reached its highest values towards the end of the D/O interstadials whereas the warmest temperature values observed in the GISP2 δ^{18}O record are found at the beginning (Cacho et al., 1999). Thus, when there is a gradual cooling in Greenland, the

Alboran Sea is still warming up. The primary productivity records show the same characteristic pattern as the $U_{37}^{k'}$-SST, involving a gradual increase towards more productive conditions towards the end of D/O interstadials reflected in TOC, total alkenone concentration and Ba$_{excess}$ records (Fig. 2). In contrast, the proxies that reflect atmospheric moisture and wind strength as well as deep-water ventilation follow the pattern of GISP2 records (Fig. 2). We explored these differences using two approaches: first, by calculating leads and lags between these proxies with a D/O periodicity (Table 3, Fig. 5) and, second, by focusing on the sequence of processes during the D/O long cycles and representing them on a time line (Table 4, Fig. 6).

The first statistical approach reveals that all primary productivity proxies show a lag with respect to SST in the time needed to reach maximum (130 ± 400 yr) and minimum values (140 ± 440 yr). However, the value of this lag varies widely between the different proxies (Fig. 5, Table 3), probably as a result of the noise introduced by secondary processes affecting each of the records. In contrast, the maximum fluvial input, marked by Al (%), leads primary productivity maxima by more than 600 years (Fig. 5, Table 3). Thus, nutrient enrichment by fluvial discharges was not the critical factor limiting primary productivity in the Alboran Sea during the glacial period; the southerly displacement of the westerly wind system that drove local upwelling in the Alboran Sea seems to have been the main influence on primary productivity changes. This hypothesis is also supported by the near opposite phase angle shown by the indicators of deep-water ventilation and primary productivity (Fig. 5), thus pointing to a close relationship between the location of the north-westerly wind system and primary productivity in the Alboran Sea. That is, strong north-westerlies in the northern basins (see Fig. 5, dashed arrows), involved minimal Alboran Sea primary productivity which increased when this wind system was displaced towards the south (Fig. 3).

Maximum aridity in southern Iberia, recorded by the down-core pollen record, preceded minimum SST by 200 ± 240 years. But the maximum lead with respect to SST is shown by the transport of Saharan dust (Si/ Si+K) which reached maximum intensity 260 ± 430 yr prior to minimum SST (Table 3). This result raises questions about the role of dust in the rapid climate change. Recently, a study carried out in the Indian monsoon region observed that the increase in dust supplied from the nearby deserts was consistent with the establishment of colder temperatures related to D/O stadial periods (Kudrass et al., 2001). This study from the Alboran record shows the occurrence of enhanced aridity and intensified Saharan winds during cold D/O periods (Moreno et al., 2002) but well before the coldest SST were attained. In the light of the time-series analyses carried out here, we suggest that low-latitude
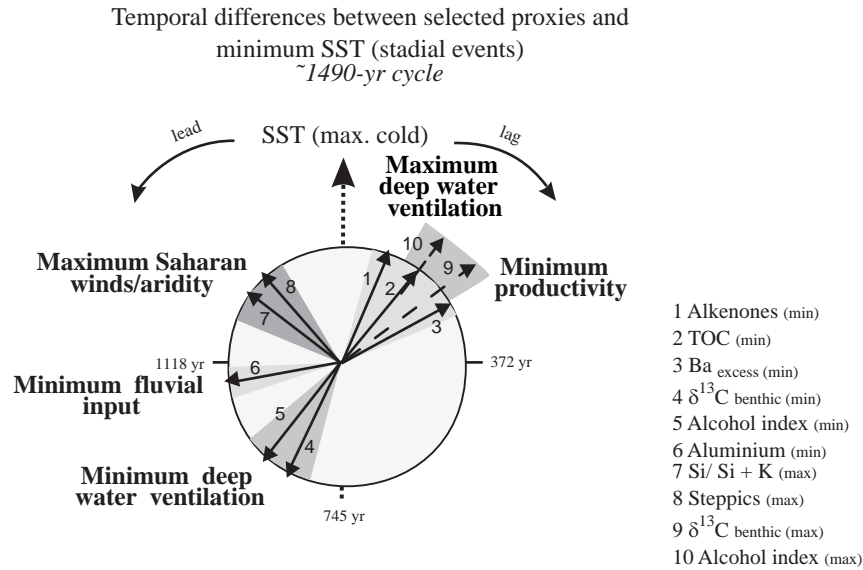
Fig. 5. Phase relationships of selected proxy records from the IMAGES core MD95-2043 during a D/O cycle (mean D/O cycles duration in the Alboran core studied is 1490 yr) where temporal evolution in reach the maximum cold is represented. See Table 3 for accurate leads and lags.

Table 4
Phase relationships of proxy records from IMAGES core MD95-2043 during the long D/O interstadials 8 and 12 calculated for the time to reach the warmest event

Variable vs. SST	Time to reach the warmest event		Average and STD
	D/O 8	D/O 12	
Ba$_{excess}$ (ppm) vs. SST	0.90	−0.20	0.35 ± 0.78
Alkenones vs. SST	−0.17	0.17	0 ± 0.24
TOC (%) vs. SST	0.70	0.17	0.43 ± 0.37
CaCO$_3$ (%) vs. SST	−0.03	0.47	0.22 ± 0.35
δ^{13}C (benthics) vs. SST	−0.58	−1.08	−0.83 ± 0.35
Alcohol index vs. SST	−0.46	−1.49	−0.98 ± 0.73
Steppics vs. SST	−1.17	−1.51	−1.34 ± 0.24
Al (%) vs. SST	−1.01	−1.61	−1.31 ± 0.42
Si/Si + K vs. SST	−0.25	−0.78	−0.52 ± 0.37

Positive values indicate that SST leads the other proxy (in kyrs). See Fig. 6 for a graphic representation.

feedback processes were involved in the forcing and transfer of millennial climatic variability.

Maximum ventilation of deep waters was acquired later, suggesting a late intensification of the high-latitude wind system. From this sequencing we infer that a lag of at least 320 yr prevailed between maximum intensity of the high-latitude (westerly) and low-latitude (Sahara) wind systems. Since some processes analyzed in the Alboran core were better represented by the D/O *long* cycles, we studied in detail the sequence of the different proxy records over a 3300-yr cycle, making statistical calculations of the leads and lags between the processes inferred through D/O interstadials 8 and 12 and their respective HEs (HE4 and HE5). In Table 4, the time to reach the warmest event was chosen to calculate the differences in the evolution of the studied processes:

primary productivity, deep-water ventilation, aridity–humidity in the continent and Saharan wind intensity with respect to SST. In Fig. 6, the main processes discussed in the context of the Alboran Sea are shown on a time line covering a D/O *long* cycle together with the climatic evolution over Greenland. Our results for the D/O longer cycles corroborate the sequence of processes described by considering every D/O event.

These findings are particularly relevant since they represent the first report of leads and lags between different latitudinal processes operating on a centennial–millennial time-scale in both oceanic and atmospheric systems. Nevertheless, since we base our hypothesis on one sedimentary core, we cannot completely rule out a potential artifact in the sedimentary signal produced by secondary processes affecting
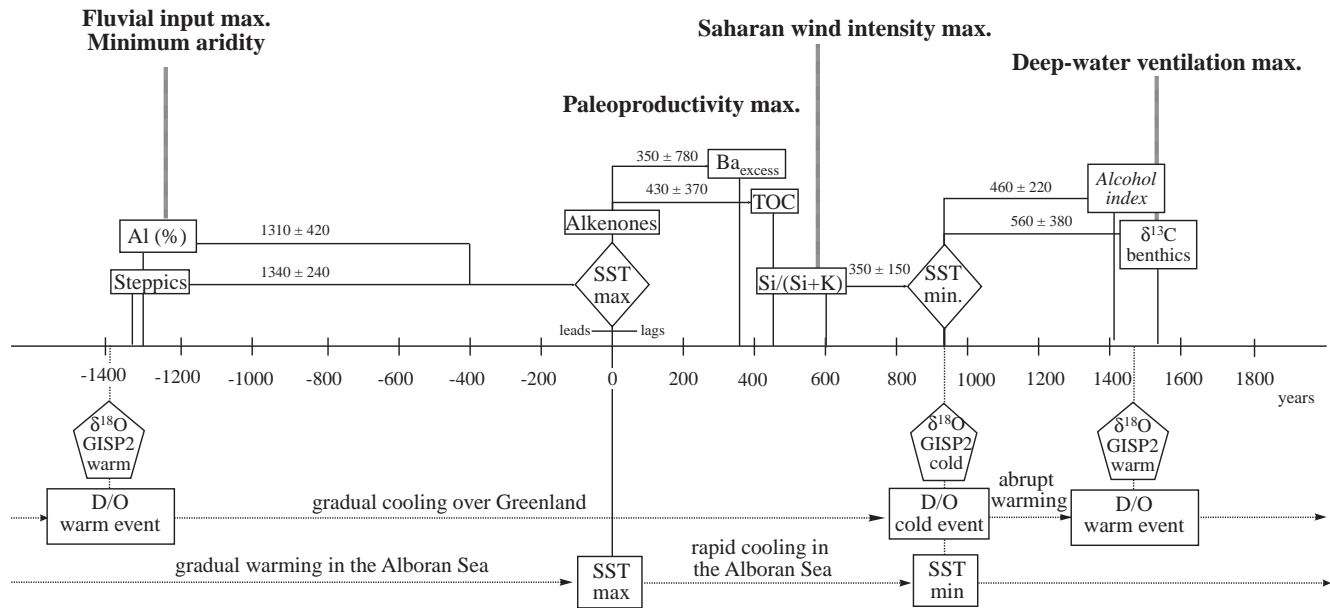
Fig. 6. Phase relationships of selected proxy records from the IMAGES core MD95-2043 during a hypothetical long D/O cycle (i.e. D/O interstadial 8 and Heinrich 4). See Table 4 for the statistical calculations. Main processes represented are indicated in bold type.

our different records. Thus, further work with similar multi-proxy approaches in different regions is needed to confirm or disprove our findings, before we go on to make further interpretations of global significance.

6. Conclusions

The Alboran core MD95-2043 provides a unique dataset comprising several proxies that record the millennial-scale variation of atmospheric and oceanic process throughout the last glacial cycle. The interpretation of the whole set of proxies in combination with similar studies performed on marine and lacustrine cores allows us to infer two different climate scenarios for the Western Mediterranean region during D/O cold stadials and warm interstadials, respectively. The position and intensity of the north-westerly belt is indicated as the main forcing mechanism to explain the variability observed.

Results on spectral analyses carried out on selected proxy profiles from the core under study reveal the presence of four significant periodicities (8000, 5000, 3300 and 1470 years) in agreement with those found in Greenland and other paleoclimatic records. Significance and also the variance controlled by each of these bands are very different between each group of the considered proxies. The 1470-yr cycle is the most significant for the records considered with the exception of those reflecting conditions on land (vegetation and Saharan dust) which showed the highest significance at the 3300 and 8000 frequency bands. The HE signal was particularly amplified in records of SST, vegetation cover and Saharan dust, as is proved by both the significance and the variance explained by the 8000 yr band. As regards the temporal leads and lags between the different proxies, we find a particularly intriguing lead in the maximum of Saharan wind transport in relation to the strength of north-westerly winds. This early response of the Saharan winds highlights the potential importance of low-latitude climatic processes in the global array of abrupt climate change.

References

Abrantes, F., 1988. Diatom productivity peak and increased circulation during the latest Quaternary in the Alboran basin (western Mediterranean). Marine Micropaleontology 13, 79–96.

Allen, J.R.M., Brandt, U., Brauer, A., Hubberten, H.W., Huntley, B., Keller, J., Kraml, M., Mackensen, A., Mingram, J., Negendank, J.F.W., Nowaczyk, N.R., Oberhänsli, H., Watts, W.A., Wulf, S., Zolitschka, B., 1999. Rapid environmental changes in southern Europe during the last glacial period. Nature 400, 740–743.

Bárcena, M.A., Cacho, I., Abrantes, F., Sierro, F.J., Grimalt, J.O., Flores, J.A., 2001. Paleoproductivity variations related to climatic conditions in the Alboran Sea (western Mediterranean) during the last glacial–interglacial transition: the diatom record. Palaeogeography, Palaeoclimatology, Palaeoecology 167 (3–4), 337–357.

Béthoux, J.P., 1979. Budgets of the Mediterranean Sea. Their dependence on the local climate and on the characteristics of the Atlantic waters. Oceanologica Acta 2, 157–163.

Bond, G., Broecker, W.S., Johnsen, S.J., McManus, J., Labeyrie, L., Jouzel, J., Bonani, G., 1993. Correlations between climate records from North Atlantic sediments and Greenland ice. Nature 365, 143–147.

Cacho, I., Grimalt, J.O., Pelejero, C., Canals, M., Sierro, F.J., Flores, J.A., Shackleton, N.J., 1999. Dansgaard–Oeschger and Heinrich event imprints in Alboran Sea temperatures. Paleoceanography 14, 698–705.

Cacho, I., Grimalt, J.O., Sierro, F.J., Shackleton, N.J., Canals, M., 2000. Evidence for enhanced Mediterranean thermohaline circulation during rapid climatic coolings. Earth and Planetary Science Letters 183, 417–420.

Cacho, I., Grimalt, J.O., Canals, M., Sbaffi, L., Shackleton, N.J., Schönfeld, J., Zahn, R., 2001. Variability of the western Mediterranean sea surface temperature during the last 25,000 years and its connection with the Northern Hemisphere climatic changes. Paleoceanography 16, 40–52.

Cacho, I., Grimalt, J.O., Canals, M., 2002. Response of the Western Mediterranean Sea to rapid climatic variability during the last 50,000 years: a molecular biomarker approach. Journal of Marine Systems 33–34, 253–272.

Combourieu Nebout, N., Turon, J.L., Zahn, R., Capotondi, L., Londeix, L., Pahnke, K., 2002. Enhanced aridity and atmospheric high-pressure stability over the western Mediterranean during the North Atlantic cold events of the past 50 k.y. Geology 30, 863–866.

Dansgaard, W., Johnsen, S.J., Clausen, H.B., Dahl-Jensen, D., Gundestrup, N.S., Hammer, C.U., Hvidberg, C.S., Steffensen, J.P., Sveinbjörnsdóttir, A.E., Jouzel, J., Bond, G., 1993. Evidence for general instability of past climate from a 250-kyr ice-core record. Nature 364, 218–220.

de Garidel-Thoron, T., Beaufort, L., Linsley, B.K., Dannenmann, S., 2001. Millennial-scale dynamics of the East Asian winter monsoon during the last 200,000 years. Paleoceanography 16, 491–502.

Ganopolski, A., Rahmstorf, S., 2001. Rapid changes of glacial climate simulated in a coupled climate model. Nature 409, 153–158.

Grootes, P., Stuiver, M., 1997. Oxygen 18/16 variability in Greenland snow and ice with 10^3- to 10^5-year time resolution. Journal of Geophysical Research 102, 26455–26470.

Hurrell, J.W., 1995. Decadal trends in the North Atlantic Oscillation: regional temperatures and precipitation. Science 269, 676–679.

Krijgsman, W., 2002. The Mediterranean: Mare Nostrum of earth sciences. Earth and Planetary Science Letters 205, 1–12.

Kudrass, H.R., Hofmann, A.W., Doose, H., Emeis, K.C., Erlenkeuser, 2001. Modulation and amplification of climatic changes in the Northern Hemisphere by the indian summer monsoon during the past 80 kyr. Geology 29, 63–69.

Leroux, M., 1993. The mobile polar high: a new concept explaining present mechanisms of meridional air-mass and energy exchanges and global propagation of paleoclimatic changes. Global Planetary Change 7, 69–93.

Leuschner, D.C., Sirocko, F., 2000. The low-latitude monsoon climate during Dansgaard–Oeschger cycles and Heinrich events. Quaternary Science Reviews 19, 243–254.

Mayewski, P.A., Meeker, L.D., Twickler, M.S., Whitlow, S., Yang, Q., Lyons, W.B., Prentice, M., 1997. Major features and forcing of high-latitude northern hemisphere atmospheric circulation using a 110,000-year-long glaciochemical series. Journal of Geophysical Research 102, 26,345–26,366.

Millot, C., 1999. Circulation in the Western Mediterranean Sea. Journal of Marine Systems 20, 423–442.

Moreno, A., Cacho, I., Canals, M., Prins, M.A., Sánchez-Goñi, M.F., Grimalt, J.O., Weltje, G.J., 2002. Saharan dust transport and high latitude glacial climatic variability: the Alboran Sea record. Quaternary Research 58, 318–328.

Moreno, A., Cacho, I., Canals, M., Grimalt, J.O., 2004. Millennial-scale variability in the productivity signal from the Alboran Sea record. Palaeogeography, Palaeoclimatology, Palaeoecology 211, 205–219.

Paillard, D., Labeyrie, L., Yiou, P., 1996. Macintosh program performs time-series analysis. Eos Transactions, AGU 77, 376.

Paterne, M., Kallel, N., Labeyrie, L., Vautravers, M., Duplessy, J.C., Rossignol-Strick, M., Cortijo, E., Arnold, E., Fontugne, M., 1999. Hydrological relationship between the North Atlantic Ocean and the Mediterranean Sea during the past 15–75 kyr. Paleoceanography 14, 626–638.

Pérez-Folgado, M., Sierro, F.J., Flores, J.A., Cacho, I., Grimalt, J.O., Zahn, R., Shackleton, N., 2003. Western Mediterranean planktonic foraminifera events and millennial climatic variability during the last 70 kyr. Marine Micropaleontology 48 (1–2), 49–70.

Perkins, H., Kinder, T., La-Violette, P., 1990. The Atlantic inflow in the Western Alboran Sea. Journal Physical Oceanography 20, 242–263.

Pinardi, N., Masetti, E., 2000. Variability of the large scale general circulation of the Mediterranean Sea from observations and modelling: a review. Palaeogeography, Palaeoclimatology, Palaeocology 158, 153–173.

Rodó, X., Baert, E., Comin, F.A., 1997. Variations in seasonal rainfall in Southern Europe during the present century: relationships with the North Atlantic Oscillation and the El Niño-Southern Oscillation. Climate Dynamics 13, 275–284.

Rohling, E.J., Hages, A., Rijk, D., Kroon, D., Zacahariasse, W.J., Esima, D., 1998. Abrupt cold spells in the Northwest Mediterranean. Paleoceanography 13, 316–322.

Roucoux, K.H., Shackleton, N.J., de Abreu, L., Schönfeld, J., Tzedakis, P.C., 2001. Combined marine proxy and pollen analyses reveal rapid Iberian vegetation response to North Atlantic millennial-scale climate oscillations. Quaternary Research 56, 128–132.

Sánchez-Goñi, M.F., Turon, J.L., Eynaud, F., Gendreau, S., 2000. European climatic response to millenial-scale changes in the atmosphere-ocean system during the last glacial period. Quaternary Research 54, 394–403.

Sánchez-Goñi, M.F., Cacho, I., Turon, J.L., Guiot, J., Sierro, F.J., Peypouquet, J.-P., Grimalt, J.O., Shackleton, N.J., 2002. Synchroneity between marine and terrestrial responses to millennial scale climatic variability during the last glacial period in the Mediterranean region. Climate Dynamics 19, 95–105.

Sirocko, F., Garbe-Schönberg, D., McIntyre, A., Molfino, B., 1996. Teleconnections between the subtropical monsoons and high-latitude climates during the last deglaciation. Science 272, 526–529.

Skinner, L., McCave, I.N., 2003. Analysis and modeling of gravity- and piston coring based on soil mechanics. Marine Geology 199, 181–204.

Sumner, G., Homar, V., Ramis, C., 2001. Precipitation seasonality in Eastern and Southern coastal Spain. International Journal of Climatology 21, 219–247.

Thomson, D.J., 1990. Time series analysis of Holocene climate data. Philosophical Transactions of the Royal Society of London A 330, 601–616.

Tzedakis, C., 1999. The last climatic cycle at Kopais, central Greece. Journal of Geological Society of London 156, 425–434.

Tzedakis, P.C., Frogley, M.R., Heaton, T.H.E., 2002. Duration of last interglacial conditions in Norwestern Grecia. Quaternary Research 58, 53–55.

Van Kreveld, S.A., Sarnthein, M., Erlenkeuser, H., Grootes, P., Jung, S., Nadeau, M.J., Pflaumann, U., Voelker, A., 2000. Potential links between surging ice sheets, circulation changes and the Dansgaard–Oeschger cycles in the Irminger Sea, 60–18 kyr. Paleoceanography 15, 425–442.

Vergnaud-Grazzini, C., Pierre, C., 1991. High fertility in the Alboran Sea since the Last Glacial Maximum. Paleoceanography 6, 519–536.

Voelker, A., 2002. Global distribution of centennial-scale records for marine isotope stage (MIS) 3: a database. Quaternary Science Reviews 21, 1185–1212.

Wanner, H., Brönnimann, S., Casty, C., Gyalistras, D., Luterbacher, J., Schmutz, C., Stephenson, D.B., Xoplaki, E., 2001. North Atlantic oscillation-concepts and studies. Surveys of Geophysics 22, 321–382.

Yiou, P., Baert, E., Loutre, M.F., 1996. Spectral analysis of climate data. Surveys of Geophysics 17, 619–663.